

# $\eta, \eta'$ photo- and electroproduction off nucleons

B. Borasoy<sup>1</sup>, E. Marco<sup>2</sup>, and S. Wetzel

Physik Department  
Technische Universität München  
D-85747 Garching, Germany

## Abstract

The photo- and electroproduction of the  $\eta, \eta'$  mesons on nucleons are investigated within a relativistic chiral unitary approach based on coupled channels. The  $s$ -wave potentials for electroproduction and meson-baryon scattering are derived from a chiral effective Lagrangian which includes the  $\eta'$  as an explicit degree of freedom and incorporates important features of the underlying QCD Lagrangian such as the axial  $U(1)$  anomaly. The effective potentials are iterated in a Bethe-Salpeter equation and cross sections for  $\eta, \eta'$  photo- and electroproduction from nucleons are obtained. The results for the  $\eta'$  photoproduction cross section on protons reproduce the appearance of an  $S_{11}$  resonance around 1.9 GeV observed at ELSA. The inclusion of electromagnetic form factors increases the predicted  $\eta$  electroproduction cross sections on the proton, providing a qualitative explanation for the hard form factor of the photocoupling amplitude observed at CLAS.

**PACS:** 11.80.-m, 12.39.Fe, 13.60.-r, 13.75.-n, 14.20.Gk

**Keywords:**  $\eta, \eta'$  electroproduction, chiral symmetry, unitarity, resonances.

---

<sup>1</sup>email: borasoy@physik.tu-muenchen.de

<sup>2</sup>email: emarco@physik.tu-muenchen.de

# 1 Introduction

Chiral symmetry is believed to govern interactions among hadrons at low energies where the relevant degrees of freedom are not the quark and gluon fields of the QCD Lagrangian, but composite hadrons. In order to make contact with experiment one must resort to methods such as chiral perturbation theory (ChPT) which incorporates the symmetries and symmetry breaking patterns of underlying QCD and is written in terms of the active degrees of freedom. A systematic loop expansion can be carried out which inherently involves a characteristic scale  $\Lambda_\chi = 4\pi F_\pi \approx 1.2$  GeV at which the chiral series is expected to break down. The limitation to very low-energy processes is even enhanced in the vicinity of resonances. The appearance of resonances in certain channels constitutes a major problem to the loopwise expansion of ChPT since their contribution cannot be reproduced at any given order of the chiral series. This can be prevented by including the resonance exchanges explicitly with the couplings fixed from electromagnetic and hadronic data. In that case, however, the theory loses its predictive power and does not provide a stringent test of chiral symmetry.

Recently, considerable effort has been undertaken to combine the effective chiral Lagrangian approach with non-perturbative methods, both in the meson-baryon sector [1, 2] and in the purely mesonic sector [3]. The combination with non-perturbative schemes have made it possible to go to energies beyond  $\Lambda_\chi$  and to generate resonances dynamically. Two prominent examples in the baryonic sector are the  $\Lambda(1405)$  and the  $S_{11}(1535)$ . The first one is an  $s$ -wave resonance just below the  $K^-p$  threshold and dominates the interaction of the  $\bar{K}N$  system. The properties of the  $\Lambda(1405)$  which appears at the correct position with the right width were reproduced remarkably well in [1, 4, 5]. A similar analysis was performed in [6] where in addition to the  $S_{11}(1535)$  the  $\Delta(1620)$  was also obtained via the inclusion of the  $\pi\pi N$  channel. The  $S_{11}(1535)$  is of particular interest since it decays very strongly into the  $\eta N$  channel and provides insight into the  $\eta N$  interaction. Applying the same formalism as in [1], the authors in [2] could generate the  $S_{11}(1535)$ , which they identify as a quasi-bound  $K\Lambda$ - $K\Sigma$  state. Information on the  $S_{11}(1535)$  was experimentally extracted from precise eta photoproduction data off protons close to threshold at MAMI (Mainz) [7] and together with an analogous electroproduction experiment performed at ELSA (Bonn) [8] the data covered the whole range of the  $S_{11}(1535)$  resonance.

In general, photoproduction of mesons is a tool to study baryonic resonances and the investigation of transitions between these states provides a crucial test for hadron models. The dominance of the  $\Delta(1232)$  in the photoproduction of pions, e.g., has allowed to extract information on its electromagnetic transition amplitudes. Because of their hadronic decay modes nucleon resonances have large overlapping widths, which makes it difficult to study individual states, but selection rules in certain decay channels can reduce the number of possible resonances. The isoscalars  $\eta$  and  $\eta'$  are such examples since, due to isospin conservation, only the isospin- $\frac{1}{2}$  excited states decay into the  $\eta N$  and  $\eta' N$  channels.

Electroproduction experiments are even more sensitive to the structure of the nucleon due to the longitudinal coupling of the virtual photon to the nucleon spin and might in addition yield some insight into the possible onset of perturbative QCD. Perturbative QCD should apply at sufficiently high photon virtuality  $Q^2 = -k^2$ , see e.g. [9, 10], however there is no consensus about how high the momentum transfer must be. It has been found experimentally, that in the case of electroproduction of the  $\Delta(1232)$  resonance at momentum transfers up to  $Q^2 = 4.0$  GeV<sup>2</sup> perturbative QCD is not applicable, [11], whereas a possible onset of scaling in the reaction

$e + p \rightarrow e + p + \eta$  at  $Q^2 = 3.6 \text{ GeV}^2$  is reported in [12]. CLAS at JLab has also electroproduced  $\eta$  mesons for invariant momentum transfers  $Q^2$  between 0.375 and 1.375  $\text{GeV}^2$  [13]. It was found that the  $S_{11}$  photocoupling  $A_{1/2}$  decreases much slower with  $Q^2$  than, e.g., the nucleon dipole form factor, which is unusual and difficult to explain theoretically.

Furthermore, there is still some controversy about the nature of the  $\eta NN$  and  $\eta' NN$  couplings. For  $\eta$  photoproduction in the  $S_{11}(1535)$  resonance region, e.g., both an effective Lagrangian approach [14] and coupled channel models [15, 16] have been employed. In these approaches the coupling of the  $\eta$  to the nucleons is described by both a pseudovector and a pseudoscalar term and the coupling constant and the coupling structure of the Born terms is unknown. In [16] it has been shown that differential cross sections are rather sensitive to the assumptions about this vertex, but within the framework of chiral perturbation theory this coupling is fixed at lowest order by making use of the chiral  $SU(3)_L \times SU(3)_R$  symmetry of the Lagrangian, whereas explicitly chiral symmetry breaking terms appear at higher orders. The  $SU(3)_L \times SU(3)_R$  symmetric limit provides therefore a convenient starting point which overcomes the problem of fixing the  $\eta NN$  vertex. The  $SU(3)$  chiral meson-baryon Lagrangian has been used in a coupled channel model [17] and by adjusting a few parameters a large amount of low-energy data was described. All the above mentioned investigations have in common that they treat the  $\eta$  meson as a pure  $SU(3)$  octet state  $\eta_8$  and mixing of  $\eta_8$  with the corresponding singlet state  $\eta_0$  which yields the physical states  $\eta$  and  $\eta'$  is neglected.

The  $\eta'$  is interesting by itself. The QCD Lagrangian with massless quarks exhibits an  $SU(3)_L \times SU(3)_R$  chiral symmetry which is broken down spontaneously to  $SU(3)_V$ , giving rise to a Goldstone boson octet of pseudoscalar mesons which become massless in the chiral limit of zero quark masses. On the other hand, the axial  $U(1)$  symmetry of the QCD Lagrangian is broken by the anomaly. The corresponding pseudoscalar singlet would otherwise have a mass comparable to the pion mass [18]. Such a particle is missing in the spectrum and the lightest candidate would be the  $\eta'$  with a mass of 958 MeV which is considerably heavier than the octet states. In conventional chiral perturbation theory the  $\eta'$  is not included explicitly, although it does show up in the form of a contribution to an LEC. However, it is also possible to include the  $\eta'$  explicitly in the chiral Lagrangian framework as has been done, e.g., in [19, 20] for the purely mesonic sector which was then extended to include baryons in [21]. Within this framework the  $\eta'$  is combined with the Goldstone bosons ( $\pi, K, \eta$ ) into a nonet and the  $\eta NN$  and  $\eta' NN$  couplings are constrained by chiral symmetry.

The  $\eta'$  photoproduction has been investigated theoretically in [22, 23, 24]. In the effective Lagrangian approach of [22] a pseudoscalar coupling of the  $\eta'$  to the nucleons was chosen and it was concluded that the  $\eta' N$  decay channel is dominated by the not so well established  $D_{13}(2080)$  resonance, whereas in the quark model used in [23] the off-shell effects of the  $S_{11}(1535)$  were prominent. In contrast, the experimental data from ELSA [25] suggested the coherent excitation of two resonances  $S_{11}(1897)$  and  $P_{11}(1986)$ . In [24]  $\eta$  and  $\eta'$  photoproduction has been studied in the coupled channel formalism working along the lines of [17]. However, the treatment of the  $\eta'$  is incomplete and only the leading terms in the meson-baryon potentials are taken into account. Their results fail to reproduce the  $\eta$  photoproduction data and are unable to describe the appearance of a  $S_{11}$  resonance for  $\eta'$  photoproduction as reported at ELSA. In order to predict the cross sections for electroproduction, which will become available from experiments at Jefferson Lab in the near future [26], a much more thorough investigation is needed.

In the present work we will focus on  $\eta, \eta'$  photo- and electroproduction off nucleons in a framework which allows a unifying description of these processes with chiral symmetry and

unitarity being the main ingredients. This is achieved by combining the effective Lagrangian with a non-perturbative scheme based on coupled channels and the Bethe-Salpeter equation. The approach contains only a few parameters, both coupling constants in the Lagrangian, so-called low-energy constants (LECs), and finite range parameters which appear in the evaluation of the loop integrals. With this small set of parameters it will be a highly non-trivial task to reproduce the data on meson photo- and electroproduction and meson-baryon scattering experiments which are described simultaneously within this multi-channel analysis. Hence this investigation will provide a test whether processes up to energies of  $\sqrt{s} \sim 2$  GeV are still constrained by chiral symmetry and whether the  $\eta'$  meson can be included in the effective Lagrangian with baryons as proposed in [21].

We will perform a global fit to a wide range of meson-baryon scattering and photoproduction data. To this end, we restrict ourselves to  $s$ -waves and therefore the comparison with data should only be valid in the near threshold region. At higher energies  $p$ -waves start dominating, as can be seen, e.g., in the work by Caro Ramon et al. [17]. One of the purposes of this work is to shed some light on the  $s$ -wave resonance  $S_{11}(1897)$  which can be studied in the  $s$ -wave approximation. Our results must be compared to the cross section reported in [25]. We will continue giving predictions for  $\eta$  and  $\eta'$  electroproduction processes and compare our results with the  $\eta$  electroproduction data from CLAS [12]. As we will see, the present framework also provides an at least qualitative explanation of the slow fall-off with increasing  $Q^2$  of the  $S_{11}(1535)$  photocoupling. Effects of  $\eta$ - $\eta'$  mixing and the importance of the  $\eta'$  contributions in this coupled channel formalism even for processes where it appears only as a virtual state are discussed in detail. This may eventually lead to a better understanding of gluonic effects and the significance of the axial  $U(1)$  anomaly in low-energy hadron physics.

In the next two sections, we introduce the effective Lagrangian and the coupled channel formalism which is then generalized to electroproduction processes. The results of our analysis are presented and compared to existing  $\eta, \eta'$  photoproduction and  $\eta$  electroproduction data in Sec. 5, where also predictions for  $\eta'$  electroproduction are made. We summarize our findings in Sec. 6.

## 2 The effective $U(3)$ Lagrangian

In this section, we will shortly review a systematic way of including the  $\eta'$  in the chiral effective Lagrangian. For details the reader is referred to [27, 28] in the purely mesonic sector or [21] the presence of baryons.

The  $U(3)_L \times U(3)_R$  chiral effective Lagrangian of the pseudoscalar meson nonet ( $\pi, K, \eta_8, \eta_0$ ) coupled to the ground state baryon octet ( $N, \Lambda, \Sigma, \Xi$ ) can be decomposed as

$$\mathcal{L} = \mathcal{L}_\phi + \mathcal{L}_{\phi B} \quad (1)$$

with the mesonic piece up to second chiral order [28]

$$\mathcal{L}_\phi = -\frac{v_0}{f_\pi^2} \eta_0^2 + \frac{f_\pi^2}{4} \langle u_\mu u^\mu \rangle + \frac{f_\pi^2}{4} \langle \chi_+ \rangle + i \frac{v_3}{f_\pi} \eta_0 \langle \chi_- \rangle \quad (2)$$

and a part  $\mathcal{L}_{\phi B}$  which describes the meson-baryon interactions [21]. At lowest order it reads

$$\begin{aligned} \mathcal{L}_{\phi B}^{(1)} = & i\langle \bar{B}\gamma_\mu[D^\mu, B] \rangle - \overset{\circ}{M} \langle \bar{B}B \rangle + iu_1 \frac{\eta_0^2}{f_\pi^2} \left( \langle [D^\mu, \bar{B}]\gamma_\mu B \rangle - \langle \bar{B}\gamma_\mu[D^\mu, B] \rangle \right) \\ & - \frac{1}{2}D \langle \bar{B}\gamma_\mu\gamma_5\{u^\mu, B\} \rangle - \frac{1}{2}F \langle \bar{B}\gamma_\mu\gamma_5[u^\mu, B] \rangle - \frac{1}{2}D_s \langle \bar{B}\gamma_\mu\gamma_5 B \rangle \langle u^\mu \rangle, \end{aligned} \quad (3)$$

where only the terms that are necessary for the present calculation are kept and  $\langle \dots \rangle$  denotes the trace in flavor space. The pseudoscalar meson nonet is summarized in  $u_\mu = iu^\dagger \nabla_\mu U u^\dagger$  with

$$U(\varphi, \eta_0) = u^2(\varphi, \eta_0) = \exp \left( \sqrt{2}i \frac{\varphi}{f_\pi} + i\sqrt{\frac{2}{3}} \frac{\eta_0}{f_\pi} \right) \quad (4)$$

where  $f_\pi \simeq 92.4$  MeV is the pion decay constant and  $\varphi$  contains the Goldstone bosons ( $\pi, K, \eta_8$ ). The covariant derivative of the meson fields includes the coupling to an external photon field

$$\nabla_\mu U = \partial_\mu U - iv_\mu U + iUv_\mu = \partial_\mu U + ie\mathcal{A}_\mu[Q, U] \quad (5)$$

with  $Q = \frac{1}{3}\text{diag}(2, -1, -1)$  being the quark charge matrix and  $\mathcal{A}_\mu$  the photon field. Explicit chiral symmetry breaking is induced via the quark mass matrix  $\mathcal{M} = \text{diag}(m_u, m_d, m_s)$  which enters in the combinations  $\chi_\pm = 2B_0(u^\dagger \mathcal{M} u^\dagger \pm u \mathcal{M} u)$  with  $B_0 = -\langle 0|\bar{q}q|0\rangle/f_\pi^2$  the order parameter of the spontaneous symmetry violation.

The second and third term of Eq. (2) appear already in conventional ChPT whereas the first and fourth one are due to the axial  $U(1)$  anomaly. The first one is the mass term of the singlet field  $\eta_0$  which remains in the chiral limit of vanishing quark masses. The coefficient  $v_0$  is a parameter not fixed by chiral symmetry and in the large  $N_c$  limit it is proportional to the topological susceptibility of Gluodynamics. The fourth term yields  $\eta_8$ - $\eta_0$  mixing, which can be described in terms of a single mixing angle, see Eq. (A.2).<sup>3</sup>

The ground state baryon octet ( $N, \Lambda, \Sigma, \Xi$ ) is summarized in a  $3 \times 3$  matrix  $B$ ,  $\overset{\circ}{M}$  is the common baryon octet mass in the chiral limit and  $D, F, D_s$  are the axial vector couplings of the baryons to the mesons. The values of  $D$  and  $F$  are extracted phenomenologically from the semileptonic hyperon decays and a fit to data delivers  $D = 0.80 \pm 0.01$ ,  $F = 0.46 \pm 0.01$  [29]. The parameters  $u_1$  and  $D_s$  do not enter in conventional ChPT and, since their values have not yet been determined, we will extract them from our fit. Finally, the covariant derivative of the baryon fields is given by

$$[D_\mu, B] = \partial_\mu B + [\Gamma_\mu, B] \quad (6)$$

with the chiral connection

$$\Gamma_\mu = \frac{1}{2}[u^\dagger, \partial_\mu u] + ie\mathcal{A}_\mu Q. \quad (7)$$

Note that there is no pseudoscalar coupling of  $\eta_0$  to the baryons of the form  $\eta_0 \bar{B}\gamma_5 B$ . Such a term is in principle possible but can be absorbed by the  $D_s$ -term in Eq. (3) by means of the equation of motion for the baryons.

---

<sup>3</sup>However, as was shown in [28], it is not the only contribution to  $\eta_8$ - $\eta_0$  since terms from the fourth order Lagrangian yield off-diagonal elements for the derivative pieces of the Lagrangian so that the mixing in the  $\eta$ - $\eta'$  system can not be parameterized in terms of a single mixing angle if large  $N_c$  counting rules are not imposed. The presentation of counterterms of the fourth order mesonic Lagrangian is beyond the scope of this work and for our purposes it will be sufficient to assume a mixing scheme in terms of one mixing parameter.

At next-to-leading order the terms relevant for  $s$ -wave meson-baryon scattering are

$$\begin{aligned}
\mathcal{L}_{\phi B}^{(2)} = & b_D \langle \bar{B} \{ \chi_+, B \} \rangle + b_F \langle \bar{B} [ \chi_+, B ] \rangle + b_0 \langle \bar{B} B \rangle \langle \chi_+ \rangle \\
& + i \frac{c_D}{f_\pi} \eta_0 \langle \bar{B} \{ \chi_-, B \} \rangle + i \frac{c_F}{f_\pi} \eta_0 \langle \bar{B} [ \chi_-, B ] \rangle + i \frac{c_0}{f_\pi} \eta_0 \langle \bar{B} B \rangle \langle \chi_+ \rangle \\
& + d_1 \langle \bar{B} \{ u_\mu, [u^\mu, B] \} \rangle + d_2 \langle \bar{B} [u_\mu, [u^\mu, B]] \rangle + d_3 \langle \bar{B} u_\mu \rangle \langle u^\mu B \rangle + d_4 \langle \bar{B} B \rangle \langle u^\mu u_\mu \rangle \\
& + d_5 \langle \bar{B} \{ u_\mu, B \} \rangle \langle u^\mu \rangle + d_6 \langle \bar{B} [u_\mu, B] \rangle \langle u^\mu \rangle + d_7 \langle \bar{B} B \rangle \langle u^\mu \rangle \langle u_\mu \rangle.
\end{aligned} \tag{8}$$

We made use of the Cayley-Hamilton identity, in order to eliminate  $\langle \bar{B} \{ u_\mu, [u^\mu, B] \} \rangle$ . The terms  $b_D, b_F, b_0$  and  $d_{1, \dots, 4}$  are already present in the  $SU(3)$  case, whereas  $c_D, c_F, c_0$  and  $d_{5, 6, 7}$  are new terms of the extended theory. The LECs  $b_D$  and  $b_F$  are responsible for the splitting of the baryon octet masses at leading order in symmetry breaking. Working in the  $SU(2)$  limit of equal  $u$  and  $d$  quark masses,  $m_u = m_d = \hat{m}$ , one obtains

$$\begin{aligned}
M_\Sigma - M_N &= 4(b_D - b_F)(m_K^2 - m_\pi^2) \\
M_\Xi - M_N &= -8b_F(m_K^2 - m_\pi^2) \\
M_\Sigma - M_\Lambda &= \frac{16}{3}b_D(m_K^2 - m_\pi^2).
\end{aligned} \tag{9}$$

Since the three baryon mass differences are represented in terms of two parameters, there is a corresponding sum rule – the Gell-Mann–Okubo mass relation for the baryon octet [30]:

$$M_\Sigma - M_N = \frac{1}{2}(M_\Xi - M_N) + \frac{3}{4}(M_\Sigma - M_\Lambda) \tag{10}$$

which experimentally has only a 3% deviation. A least-squares fit to the mass differences (9) yields  $b_D = 0.066 \text{ GeV}^{-1}$  and  $b_F = -0.213 \text{ GeV}^{-1}$ . The  $b_0$  term, on the other hand, cannot be determined from the masses alone. One needs further information which is provided by the pion-nucleon  $\sigma$ -term and reads at leading order

$$\sigma_{\pi N} = \hat{m} \langle N | \bar{u}u + \bar{d}d | N \rangle = -2m_\pi^2(b_D + b_F + 2b_0). \tag{11}$$

Employing the empirical value of [31],  $\sigma_{\pi N} = 45 \pm 8 \text{ MeV}$ , one obtains  $b_0 = -0.52 \pm 0.10 \text{ GeV}^{-1}$ . Recently, this value has been questioned [32] and the authors of this work arrive at a value  $\sigma_{\pi N} = 60 \pm 7 \text{ MeV}$  which would translate into a value of  $b_0 = -0.71 \pm 0.09 \text{ GeV}^{-1}$ . In particular the latter value yields a large strangeness content of the proton, however both values may change if loop effects are included [33]. Due to these uncertainties in the value of  $b_0$ , any fitted value which lies in the range  $-0.80 \text{ GeV}^{-1} < b_0 < -0.20 \text{ GeV}^{-1}$  is still acceptable. In the  $U(3)$  formalism three more explicitly symmetry breaking terms enter,  $c_D, c_F$  and  $c_0$ , which have unknown values. These are suppressed by one order of  $1/N_c$  with respect to their counterparts  $b_D, b_F$  and  $b_0$ , and following  $1/N_c$  arguments one can assume them to be significantly smaller in magnitude, e.g.  $|c_0| \ll |b_0|$ . We will vary these three parameters only within small ranges around zero and compare the results with existing data.

The situation is less clear for the derivative terms  $d_1, \dots, d_7$ . In [17] the parameters  $d_1$  to  $d_4$  were determined in a coupled channel analysis while being subject to two constraints from  $\pi N$  and  $KN$  scattering lengths. The authors obtain the values  $d_1 = -0.20$ ,  $d_2 = 0.22$ ,  $d_3 = 0.42$  and  $d_4 = -1.62$  in units of  $\text{GeV}^{-1}$ . However, they employ the  $SU(3)$  chiral Lagrangian which does not include the  $\eta'$  explicitly and work in the heavy baryon formulation treating the baryons as

heavy sources while loop diagrams are regularized by an explicit cutoff. We expect the values of  $d_1, \dots, d_4$  to change in our approach since we derive the potentials from the relativistic  $U(3)$  Lagrangian and the loops are evaluated in dimensional regularization. An estimate for the parameters  $d_{1,\dots,7}$  can alternatively be obtained by assuming resonance saturation. Within this model the decuplet  $T$  of spin- $\frac{3}{2}$  baryon fields which includes the  $\Delta(1232)$  is expected to determine approximately the values of the  $d_{1,\dots,7}$  parameters. The interaction of the decuplet states with the octet baryons and the pseudoscalar mesons reads at lowest order

$$\mathcal{L}_{TB\phi} = \frac{\mathcal{C}}{2} \bar{T}_\mu u^\mu B + h.c. \quad (12)$$

where the coupling constant  $|\mathcal{C}| = 1.2\text{--}1.8$  can be determined from the decays  $T \rightarrow B\pi$ . The decuplet contributions to the LECs  $d_{1,\dots,7}$  yield at leading order in the averaged decuplet mass  $M_\Delta$  via resonance saturation the values  $d_1 = -0.27$ ,  $d_2 = 0.09$ ,  $d_3 = 0.27$ ,  $d_4 = -0.27$ ,  $d_5 = 0$ ,  $d_6 = 0.18$  and  $d_7 = 0.09$  in units of  $\text{GeV}^{-1}$  for  $|\mathcal{C}| = 1.5$  and  $M_\Delta = 1.38$  GeV. While  $d_{1,2,3}$  are in qualitative agreement with the fitted values from [17], the values for  $d_4$  differ considerably. Contributions from other resonances have been neglected here since we are only interested in a rough order of magnitude estimate for these parameters. We will therefore vary  $d_i$ ,  $i = 1, 2, 3, 5, 6, 7$ , within small ranges around the values. Most unknown couplings are constrained within certain ranges and they will be fixed from a fit to many scattering data. After setting up the Lagrangian which we will be using in this work, we can now proceed by explaining our coupled channel approach.

### 3 The coupled channel approach

The Lagrangian of the preceding section could in principle be used to calculate the one-loop diagrams of  $\eta'$  electroproduction, but the perturbative expansion of the chiral series will be useless for this case. First, the  $\eta'$  with a mass of 958 MeV close to the scale of chiral symmetry breaking  $\Lambda_\chi \approx 1.2$  GeV introduces a new massive scale in the effective theory which spoils the strict chiral counting scheme unless one imposes large  $N_c$  counting rules [27]<sup>4</sup>. Large  $N_c$  counting rules in turn imply that the  $\eta'$  mass must be treated as a small quantity. In our opinion, this assumption is phenomenologically not justified and we consider the  $\eta'$  to be a massive state. Second,  $\eta'$  electroproduction has a threshold close to  $\sqrt{s} \approx 2$  GeV far beyond the scale  $\Lambda_\chi \approx 1.2$  GeV at which the perturbative chiral expansion is expected to break down. One must therefore resort to non-perturbative schemes.

For the investigation of hadronic resonances the combination of the effective chiral Lagrangian with coupled channel approaches have been proven to be useful. E.g., in [2] the  $S_{11}(1535)$  nucleon resonance emerged as a quasi-bound state of  $K\Lambda$  and  $K\Sigma$ . In the present investigation, we employ a relativistic chiral unitary approach based on coupled channels. By imposing constraints from unitarity we perform the resummation of the amplitudes obtained from the tree level potentials and the loop integrals. Let us describe first the coupled channel approach for meson-baryon scattering, which will then be generalized to electroproduction of

---

<sup>4</sup>For specific processes such as the dominant hadronic decay mode of the  $\eta'$ ,  $\eta' \rightarrow \eta\pi\pi$ , it has been shown that the usage of infrared regularization yields a well-behaved chiral series since loops with an  $\eta'$  are suppressed [34]

mesons. To this end, one expands  $u_\mu$  and  $\Gamma_\mu$  in Eqs. (2), (7) in terms of the mesons

$$u_\mu = -\frac{2}{f_\pi} \partial_\mu \varphi - \frac{1}{f_\pi} \sqrt{\frac{2}{3}} \partial_\mu \eta_0 + \dots, \quad (13)$$

$$\Gamma_\mu = \frac{1}{2f_\pi^2} [\varphi, \partial_\mu \varphi] + \dots \quad (14)$$

In our model the relativistic tree level amplitude  $V_\alpha^\beta$  for the meson-baryon scattering process  $B_a \phi_i \rightarrow B_b \phi_j$  is obtained by the diagrams shown in Fig. (1).

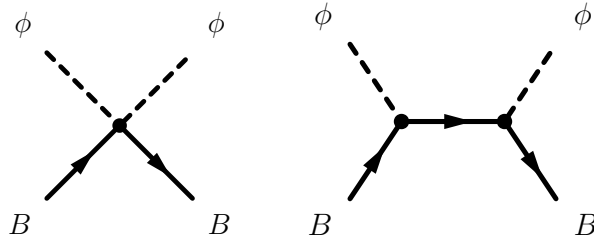


Figure 1: Contact interaction and Born direct term for meson-baryon scattering. Solid and dashed lines denote the baryons and pseudoscalar mesons, respectively.

In the present work, we restrict ourselves to the  $s$ -wave partial wave amplitude  $V$  which is given by

$$V(s) = \frac{1}{8\pi} \sum_{\sigma=1}^2 \int d\Omega T(s, \Omega; \sigma) \quad (15)$$

where we have averaged over the spin  $\sigma$  of the baryons and  $s$  is the invariant energy squared. It is most convenient to work in the isospin basis and to characterize the meson-baryon states in the electroproduction process  $\gamma N \rightarrow \phi B$  by their total isospin  $I = 1/2$  or  $I = 3/2$ . The analysis reduces then to five channels with total isospin  $I = 1/2$  which are  $|\pi N\rangle^{(1/2)}$ ,  $|\eta N\rangle^{(1/2)}$ ,  $|K\Lambda\rangle^{(1/2)}$ ,  $|K\Sigma\rangle^{(1/2)}$ ,  $|\eta' N\rangle^{(1/2)}$  (labeled with indices 1, 2, 3, 4, 5, respectively) and two channels with  $I = 3/2$ ,  $|\pi N\rangle^{(3/2)}$ ,  $|K\Sigma\rangle^{(3/2)}$  (labeled by indices 6 and 7). The potentials read

$$V_\alpha^\beta = \frac{N_a N_b}{f_\pi^2} C_\alpha^\beta \quad (16)$$

where  $\alpha$  and  $\beta$  label the channels involved and  $N_{a(b)} = \sqrt{E_{a(b)} + M_{a(b)}}$  and  $E_{a(b)}$ ,  $M_{a(b)}$  are the energy and mass of the incoming (outgoing) baryon. Note that we have replaced the common baryon octet mass  $\overset{\circ}{M}$  by the physical masses  $M_{a(b)}$  which is consistent at the order the potentials  $V$  are calculated and use of the physical masses is also mandatory in order to reproduce the correct threshold positions of the different channels involved. The coefficients  $C_\alpha^\beta(s)$  are given in App. A.

For each partial wave  $l$  unitarity imposes a restriction on the (inverse)  $T$ -matrix above the pertinent thresholds

$$\text{Im} T_l^{-1} = -\frac{|\mathbf{q}_{cm}|}{8\pi\sqrt{s}} \quad (17)$$



with  $\mathbf{q}_{cm}$  being the three-momentum in the center-of-mass frame of the channel under consideration. Hence the imaginary part of  $T^{-1}$  is similar to the imaginary piece of the fundamental scalar loop integral  $\tilde{G}$  above threshold

$$\tilde{G}(q^2) = \int \frac{d^d l}{(2\pi)^d} \frac{i}{[(q-l)^2 - M_B^2 + i\epsilon][l^2 - m_\phi^2 + i\epsilon]} \quad (18)$$

with  $M_B$  and  $m_\phi$  being the physical masses of the baryon and the meson, respectively. For the finite part,  $G$  of  $\tilde{G}$ , one obtains, e.g., in dimensional regularization

$$G(q^2) = \frac{1}{32\pi^2 q^2} \left\{ q^2 \left[ \ln\left(\frac{m_\phi^2}{\mu^2}\right) + \ln\left(\frac{M_B^2}{\mu^2}\right) - 2 \right] + (m_\phi^2 - M_B^2) \ln\left(\frac{m_\phi^2}{M_B^2}\right) - 8\sqrt{q^2} |\mathbf{q}_{cm}| \operatorname{artanh} \left( \frac{2\sqrt{q^2} |\mathbf{q}_{cm}|}{(m_\phi + M_B)^2 - q^2} \right) \right\} \quad (19)$$

where  $\mu$  is the regularization scale. We allow this scale to vary for the different loops, in order to simulate higher order contributions. Alternatively, in [5, 6] the real piece has been adjusted by introducing a scale dependent constant for each channel in analogy to a subtraction constant of a dispersion relation for  $T^{-1}$ . In a more general way, one could model the real parts by taking any analytic function in  $s$  and the baryon and meson masses. This option has been successfully applied for the case of  $SU(2)$  ChPT in [37], but a straightforward generalization to the  $U(3)$  case would introduce a number of unknown new parameters and thus reduce the predictive power of the present approach.

The inverse of the amplitude  $T^{-1}$  can be decomposed into real and imaginary parts

$$T^{-1} = \tau^{-1} + G \quad (20)$$

where  $\tau$  and  $\operatorname{Re}[G]$  give the real part and  $\operatorname{Im}[G]$  gives the imaginary part required by unitarity, Eq. (17). Inverting (20) yields

$$T = [1 + \tau \cdot G]^{-1} \tau \quad (21)$$

which is understood to be a matrix equation. The matrix  $G$  is diagonal and includes the expressions for the loop integrals in each channel. Expanding expression (21)

$$T = \tau - \tau \cdot G \cdot \tau \dots \quad (22)$$

and from matching to our tree level amplitude it follows

$$\tau = V. \quad (23)$$

Our final expression for the  $T$  matrix reads then

$$T = [1 + V \cdot G]^{-1} V \quad (24)$$

which amounts to a summation of a bubble chain in the  $s$ -channel. This is equivalent to a Bethe-Salpeter equation with  $V$  as potential.

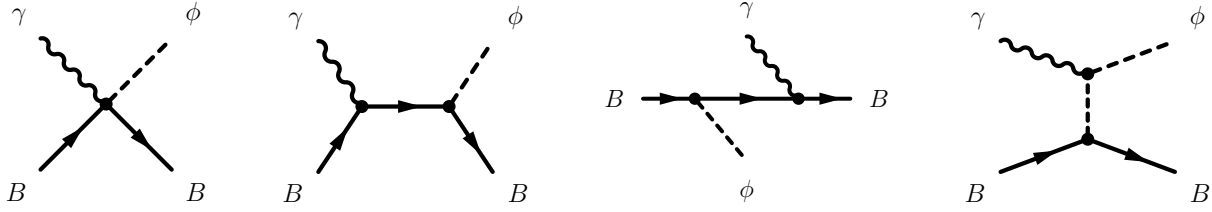


Figure 2: Contact interaction, Born terms in the  $s$ - and  $u$ -channel and meson pole diagram for meson electroproduction. Solid and dashed lines denote the baryons and pseudoscalar mesons, respectively. The photon is represented by a wavy line.

## 4 Extension to photo- and electroproduction

We are now in a position to extend the above developed formalism to electroproduction processes. Following [17] we assume that the  $s$ -wave electroproduction process can be described by a similar Bethe-Salpeter equation as for the strong interactions. Our starting point are the contact, Born and meson-pole diagrams for meson electroproduction with vertices of the Lagrangian as presented in Sec. 2, see Fig. 2. From these diagrams we extract the transverse and longitudinal  $s$ -wave multipoles at leading order which are identified with the electroproduction potentials  $B_{0+}$  and  $C_{0+}$ , respectively. For the proton the expressions  $B_{0+}$  in the isospin basis, which can be obtained from the formulas appearing for example in [38], read

$$\begin{aligned}
B_{0+}^{(1)} &= (D + F)(2R^{(1)} - S^{(1)}) \\
B_{0+}^{(2)} &= -\left(\sqrt{2}(2D + 3D_s) \sin \vartheta + (D - 3F) \cos \vartheta\right) S^{(2)} \\
B_{0+}^{(3)} &= (D + 3F)R^{(3)} \\
B_{0+}^{(4)} &= (D - F)(R^{(4)} - 2S^{(4)}) \\
B_{0+}^{(5)} &= \left(\sqrt{2}(2D + 3D_s) \cos \vartheta - (D - 3F) \sin \vartheta\right) S^{(5)} \\
B_{0+}^{(6)} &= \sqrt{2}(D + F)(R^{(6)} + S^{(6)}) \\
B_{0+}^{(7)} &= -\sqrt{2}(D - F)(R^{(7)} + S^{(7)}).
\end{aligned} \tag{25}$$

where  $\vartheta$  is the mixing angle (see the Appendix). The functions  $R^{(\alpha)}$  and  $S^{(\alpha)}$  for the electroproduction process  $\gamma B_a \rightarrow \phi B_b$  in the channel  $\alpha$  are given by

$$\begin{aligned}
R^{(\alpha)} &= \frac{e(M_a + M_b)N_a}{64\pi f_\pi \sqrt{3s} |\mathbf{k}|^2 N_b} \left( \frac{4N_b^2 |\mathbf{k}|^2}{M_a + \sqrt{s}} + k^2 - 2E_\phi k_0 \right. \\
&\quad \left. - \frac{1}{4|\mathbf{k}||\mathbf{q}|} [(k^2 - 2E_\phi k_0)^2 - 4|\mathbf{k}|^2 |\mathbf{q}|^2] \ln \frac{2E_\phi k_0 - 2|\mathbf{k}||\mathbf{q}| - k^2}{2E_\phi k_0 + 2|\mathbf{k}||\mathbf{q}| - k^2} \right)
\end{aligned} \tag{26}$$

$$\begin{aligned}
S^{(\alpha)} = & \frac{e(M_a + M_b)N_a}{64\pi f_\pi \sqrt{3s} |\mathbf{k}|^2 N_b} \left( m_\phi^2 + M_a^2 - M_b^2 - 2E_a E_\phi \right. \\
& + \frac{2|\mathbf{k}|^2}{N_a^2 (M_a + \sqrt{s})} \left[ (M_a + \sqrt{s})^2 - 2N_a^2 N_b^2 \right] \\
& + \frac{1}{4|\mathbf{k}||\mathbf{q}|} \left( (M_a^2 - M_b^2 - 2E_a E_\phi + m_\phi^2)^2 + 4|\mathbf{k}|^2 ((\sqrt{s} - M_a)(E_b + M_b) - |\mathbf{q}|^2) \right. \\
& \quad \left. + \frac{2|\mathbf{k}|^2}{N_a^2} (\sqrt{s} + M_a)(M_a^2 - M_b^2 - 2E_a E_\phi + m_\phi^2) \right) \\
& \quad \left. \times \ln \frac{M_b^2 - M_a^2 - m_\phi^2 + 2E_a E_\phi + 2|\mathbf{k}||\mathbf{q}|}{M_b^2 - M_a^2 - m_\phi^2 + 2E_a E_\phi - 2|\mathbf{k}||\mathbf{q}|} \right) \quad (27)
\end{aligned}$$

with  $\mathbf{k}, \mathbf{q}$  the three-momenta of the photon and the meson in the center-of-mass frame. The energies of the baryons and meson are given by  $E_{a(b)}$  and  $E_\phi$ , respectively, whereas  $M_{a(b)}$  and  $m_\phi$  denote their masses. The function  $R^{(\alpha)}$  describes charged meson electroproduction processes on protons, whereas  $S^{(\alpha)}$  is obtained when neutral mesons are produced. In the case of the neutron one obtains

$$\begin{aligned}
B_{0+}^{(1)} &= -2(D + F)(R^{(1)} + S^{(1)}) \\
B_{0+}^{(4)} &= 2(D - F)(R^{(4)} + S^{(4)}) \\
B_{0+}^{(6)} &= -\sqrt{2}(D + F)(R^{(6)} + S^{(6)}) \\
B_{0+}^{(7)} &= \sqrt{2}(D - F)(R^{(7)} + S^{(7)}) \\
B_{0+}^{(2)} &= B_{0+}^{(3)} = B_{0+}^{(5)} = 0. \quad (28)
\end{aligned}$$

The expressions for the longitudinal  $s$ -wave potentials  $C_{0+}$  have a similar structure, but are much more lengthy and will therefore not be presented for brevity.

Once a meson and a baryon have been electroproduced, they may rescatter into all possible meson-baryon pairs, as shown in Figs. 3 and 4. We sum this infinite interaction chain in the Bethe-Salpeter approach to obtain the final results for the electric dipole amplitude  $E_{0+}$  and the longitudinal  $s$ -wave  $L_{0+}$ . This procedure ensures that the resonances that appear in meson electroproduction are the same ones that appear in meson-baryon scattering. The electric

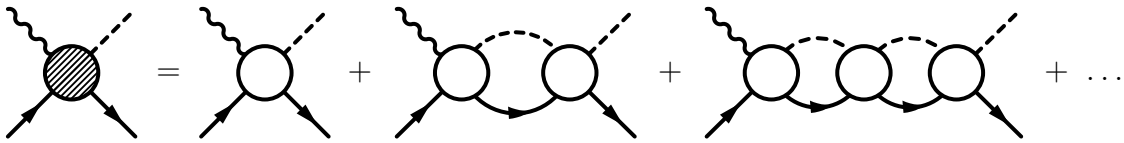


Figure 3: The  $s$ -wave electroproduction amplitude is the result of the tree level electroproduction potentials plus the diagrams where the final meson-baryon pair are rescattered. The empty circles denote either the  $s$ -wave potentials  $B_{0+}, C_{0+}$  for electroproduction or the meson-baryon scattering potentials  $V$ .

dipole moment  $E_{0+}$  is given by

$$E_{0+} = [1 + V \cdot G]^{-1} B_{0+}, \quad (29)$$

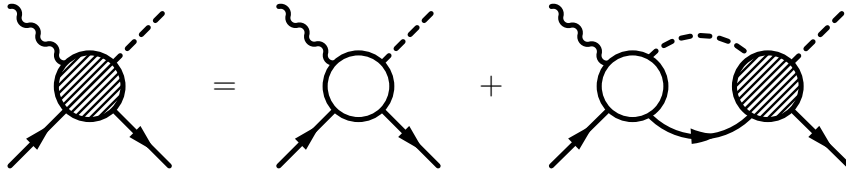


Figure 4: The iterated sum of diagrams in Fig. 3 is illustrated in compact form.

while the longitudinal  $s$ -wave  $L_{0+}$  reads

$$L_{0+} = [1 + V \cdot G]^{-1} C_{0+}. \quad (30)$$

The total cross section for the electroproduction of mesons on the nucleon is

$$\sigma_{tot} = 8\pi \frac{\sqrt{s}|\mathbf{q}|}{s - M_N^2} (|E_{0+}|^2 + \epsilon_L |L_{0+}|^2), \quad (31)$$

with  $\epsilon_L = -4\epsilon s k^2 (s - M_N^2 + k^2)^{-2}$  where  $\epsilon$  is the virtual photon polarization.

Within this formalism the baryons and mesons are treated as pointlike particles. However, with increasing momentum transfers the composite structure of hadrons will become important, affecting the  $Q^2$  behavior of the initial electroproduction potentials  $B_{0+}$  and  $C_{0+}$ . In order to analyze these effects, we will compare in the next section the results for pointlike particles with those for composite hadrons by inserting monopole form factors in  $B_{0+}$  and  $C_{0+}$ .

## 5 Results

In this section we will present the results of our calculation. We start by performing a global fit to available data for meson-proton and photon-proton reactions which constrains the parameters in the approach. This allows us to give predictions for further processes such as the cross sections for  $\pi^- p \rightarrow \eta' n$  and  $\eta$  and  $\eta'$  electroproduction. We conclude this section by studying the effects of  $\eta$ - $\eta'$  mixing and the contributions of the  $\eta'$  meson to those reactions where it is not produced as a final particle.

### 5.1 Fit to the data

We have performed a global fit to a large amount of data, consisting of meson-proton and photon-proton reactions for values of  $\sqrt{s}$  between 1.5 and 2.0 GeV. Our cross sections include only  $s$ -wave contributions, which are dominant in this energy range for most processes. From comparison with the work of [17] we expect  $p$ -waves to exceed the  $s$ -wave contribution for most processes at high energies, further away from threshold, but for a few channels they constitute the main contribution in the whole energy domain. This explains why our results are below the experimental data for some of the discussed processes.

The fit yields the values  $u_1 = -0.0125$  and  $D_s = -0.38$  for the unknown parameters of the leading order Lagrangian, Eq. (3),  $b_D = 0.066 \text{ GeV}^{-1}$ ,  $b_F = -0.185 \text{ GeV}^{-1}$  and  $b_0 = -0.250 \text{ GeV}^{-1}$  for the mass counterterms, and  $d_1 = -0.20$ ,  $d_2 = 0.10$ ,  $d_3 = 0.28$ ,  $d_4 = -0.25$ ,  $d_5 = -0.01$ ,  $d_6 = 0.075$  and  $d_7 = 0.075$  (in units of  $\text{GeV}^{-1}$ ) for the derivative couplings in the next-to-leading order Lagrangian. For the regularization scales our fitted values are  $\mu_{\pi N} = 0.30 \text{ GeV}$ ,

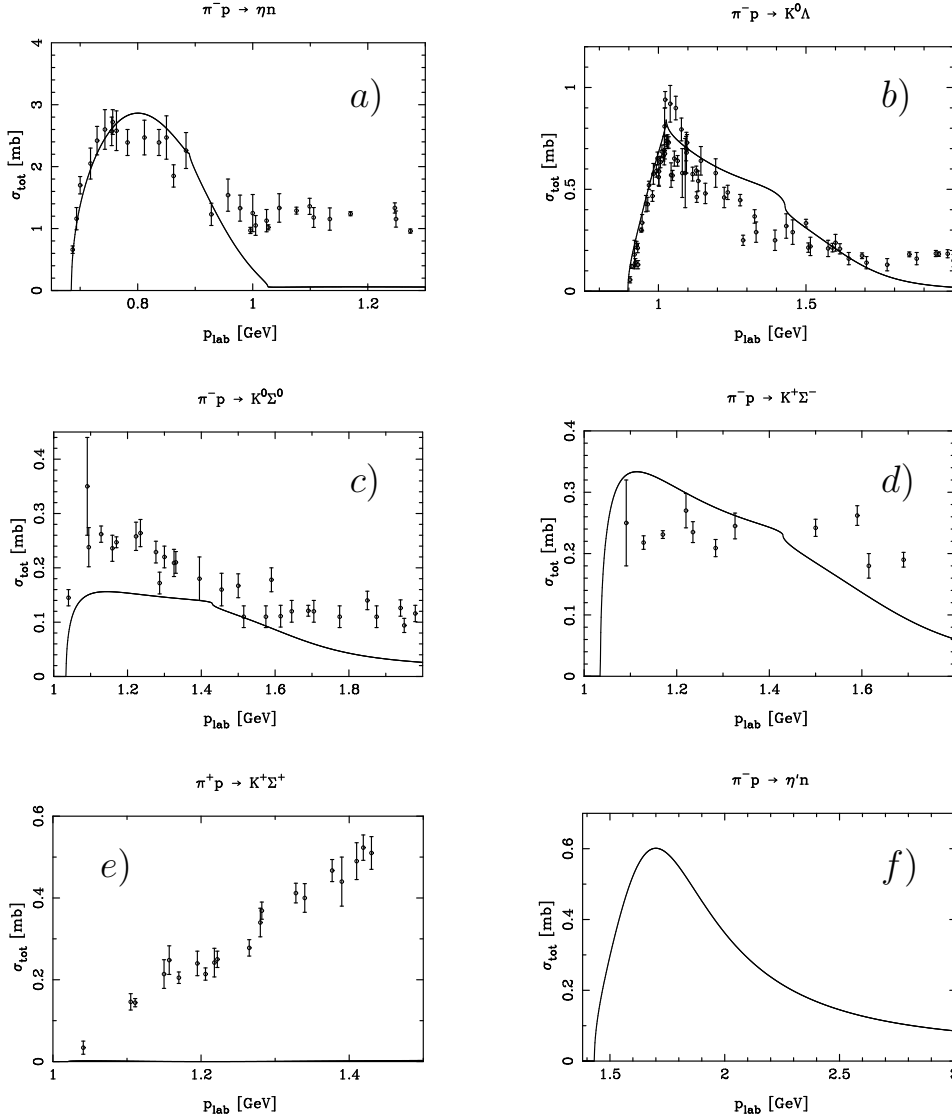


Figure 5: Total cross sections for pion-proton collision processes. The data are taken from [39].

$\mu_{\eta N} = 0.77$  GeV,  $\mu_{K\Lambda} = 0.14$  GeV,  $\mu_{K\Sigma} = 1.20$  GeV and  $\mu_{\eta'N} = 0.40$  GeV. The parameters  $c_D, c_F$  and  $c_0$  are set to zero, since according to large  $N_c$  estimates they are expected to be suppressed and small variations of their values around zero have not shown any substantial impact on the cross sections.

The pion-proton cross sections are summarized in Fig. 5: Fig. 5.a shows the cross section for the reaction  $\pi^- p \rightarrow \eta n$ . At  $p_{\text{lab}}$  energies below 1 GeV the cross section is dominated by the  $s$ -wave resonance  $S_{11}(1535)$ , which is nicely reproduced in our calculation. In Fig. 5.b the results for the reaction  $\pi^- p \rightarrow K^0 \Lambda$  are given. Again the cross section is dominated by  $s$ -waves, but in this case the main contribution stems from the  $S_{11}(1650)$  which is accompanied by a cusp effect due to the opening of the  $K\Sigma$  threshold. In Figs. 5.c and 5.d the  $K\Sigma$  production reactions are depicted. They receive some (small) contribution from the isospin  $T = 3/2$  component of the amplitude and are dominated in the low-energy region by  $s$ -wave contributions, but do not

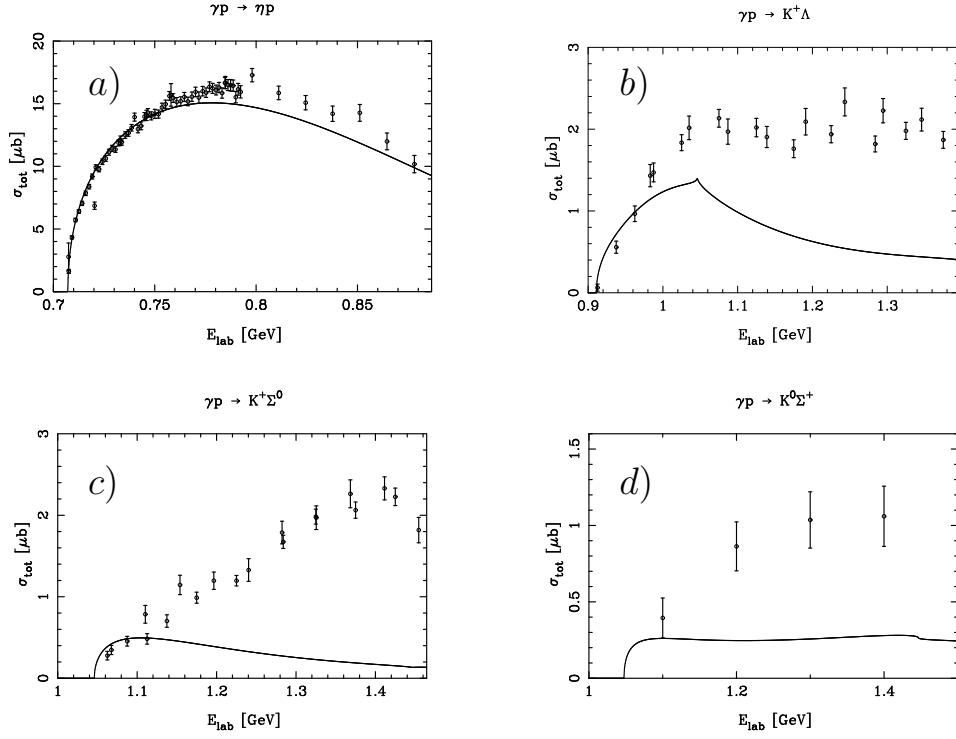


Figure 6: Shown are the total cross sections for  $\eta$  and kaon photoproduction off the proton. The data are taken from [7, 8, 40, 41].

signal the appearance of a resonance. In Fig. 5.e we show the cross section for the reaction  $\pi^+ p \rightarrow K^+ \Sigma$ . This reaction receives only contributions from the isospin  $T = 3/2$  amplitude, and it turns out that the  $s$ -wave contribution is negligible as already observed in [17]. The last pion-proton cross section is shown in Fig. 5.f, where the  $\eta'$  is produced in  $\pi^- p$  collisions. Albeit we show this plot with the rest of the pion-proton cross sections, it is important to note that the last reaction is *not* included in our fit. Once the involved parameters are constrained by the other reactions, our model provides a prediction for this process which can be checked by future experiments.

Let us now turn to the photoproduction cross sections which are shown in Fig. 6. We present in Fig. 6.a the  $\eta$  photoproduction data measured at MAMI [7] and ELSA [8] and our fitted result confirms the dominance of the  $S_{11}(1535)$ , which is responsible for almost the entire cross section in the low-energy region. Results for the reaction  $\gamma p \rightarrow K^+ \Lambda$  are given in Fig. 6.b, where at low energies the cross section is dominated by the  $S_{11}(1650)$ , while  $p$ -waves become important for  $E_{\text{lab}}$  energies above 1.1 GeV. One also observes a cusp effect due to the  $K\Sigma$  threshold. For the next two reactions,  $K^+ \Sigma^0$  and  $K^0 \Sigma^+$  photoproduction, the cross sections are  $p$ -wave dominated, and our results are able to account for small  $s$ -wave cross sections, describing the data only in the very near threshold region. Finally, we show in Fig. 7 our results for the reaction  $\gamma p \rightarrow \eta' p$ , which has been measured at ELSA [25], where the coherent contribution of two resonances, the  $S_{11}(1897)$  and  $P_{11}(1986)$ , was observed. Our formalism is capable of reproducing the appearance of an  $s$ -wave resonance around 1900 GeV in contradistinction to the work reported in [24] which remains far below the measured decay rates.

So far, we have discussed –with the exception of  $\pi^- p \rightarrow \eta' n$  in Fig. 5.f– only the channels that were used in order to constrain the undetermined chiral parameters in our approach. Using

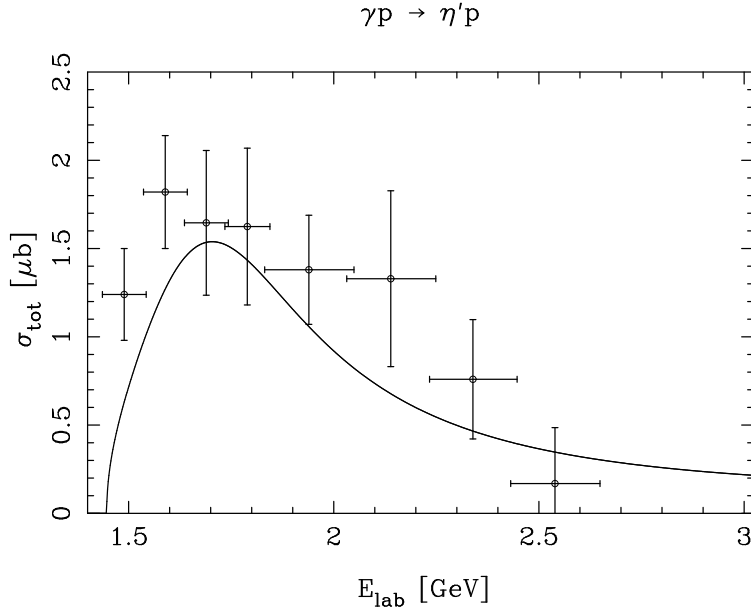


Figure 7: Given is the total cross section for  $\eta'$ -photoproduction of the proton and the data are taken from [25].

the same values for the parameters we can now predict the cross sections for further processes which will provide a true test for the applicability of the model. The electroproduction of  $\eta$  and  $\eta'$  mesons on a nucleon, e.g., is an ideal testing ground for the approach, being much more sensitive to its details.

## 5.2 Electroproduction of $\eta$ and $\eta'$ mesons

Detailed information about the electromagnetic structure of the nucleon is supplied by electroproduction experiments, which yield important constraints for hadron models. After having fixed the parameters in our approach, we can now compare our predictions for  $\eta$  and  $\eta'$  electroproduction with available experimental data. We first show our predictions for pointlike hadrons. The  $\eta$  electroproduction on the proton has been measured in detail at CLAS at JLab [13] and the data is shown together with our results in Fig. 8.a.

The invariant momentum transfer  $Q^2$  of the presented data ranges from 0.375 to 0.875 GeV<sup>2</sup> and the applicability of our approach to such high momentum transfers may be regarded as questionable. Nevertheless, we should be able to capture qualitative features of the  $Q^2$  evolution of the cross section, in particular its slow fall-off which is unusual and in sharp contrast, e.g., to the fall given by a nucleon dipole form factor. Our results, although showing less decrease with  $Q^2$  than that of a simple nucleon dipole form factor, produce a faster reduction at low  $Q^2$  than the experimental data, and then flatten at higher momentum transfers. We employed in all plots a virtual photon polarization of  $\epsilon = 0.5$  which is roughly the average of the polarizations of the CLAS experiment and small variations around this value yield changes that are almost negligible.

Our predictions for electroproduction of the  $\eta'$  on the proton are depicted in Fig. 8.b for the same range of momentum transfers and data for this process will soon become available from experiments at Jefferson Lab [26]. In this case, the features of the  $Q^2$  evolution of the cross

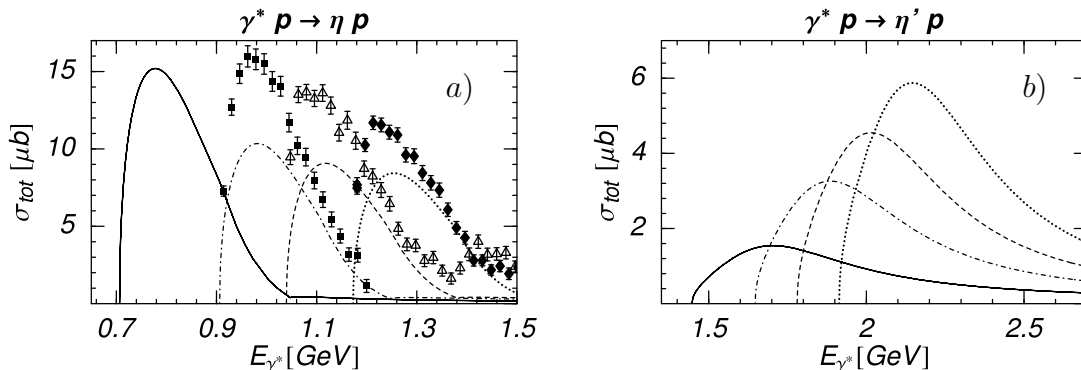


Figure 8: Cross sections for  $\eta$  and  $\eta'$  electroproduction on the proton for various invariant momentum transfers  $Q^2$ . The different lines refer to the following values of  $Q^2$ : solid line: photoproduction ( $Q^2 = 0$ ); dash-dotted line and squares:  $Q^2 = 0.375 \text{ GeV}^2$ ; dashed line and triangles:  $Q^2 = 0.625 \text{ GeV}^2$ ; dotted line and diamonds:  $Q^2 = 0.875 \text{ GeV}^2$ . The data for  $\eta$  electroproduction with the same  $Q^2$  values are taken from [13], and only statistical errors are shown.

section are even more striking, since they exhibit a fast increase instead of the usual decrease.

As already mentioned in Sec. 4, the composite structure of baryons and mesons will become increasingly important with rising invariant momentum transfers  $Q^2$ . It is therefore natural to include form factors in the initial electroproduction potentials  $B_{0+}$  and  $C_{0+}$ , in order to account for the electromagnetic structure of hadrons. One may be inclined to multiply the potentials by an overall form factor which is the same for all hadrons that interact with the photon (and thus the same for all channels). Obviously, this would reduce all electroproduction cross sections, e.g., it would be easy to produce a decreasing  $Q^2$  evolution of the  $\eta'$  electroproduction cross section, in accordance with other electroproduction processes. However, this procedure will also yield smaller cross sections for  $\eta$  electroproduction leading to stronger disagreement with the data. In this case, the inclusion of form factors which accounts for the electromagnetic structure of the baryons and mesons seems to worsen the situation.

As we will see now, there is indeed a way of including form factors for the particles, while at the same time improving the situation *both* for  $\eta$  and  $\eta'$  electroproduction. Based on the observation that form factors provide a more realistic description of the electromagnetic response of hadrons, we will present a plausible qualitative explanation for the unusually hard transition form factor of the  $S_{11}(1535)$ . This hard form factor has been difficult to understand theoretically, and only recent work within a constituent quark model using a hypercentral potential led to better agreement with experiment [42]. At the same time, it has been claimed that the hard form factor is in contrast to models that interpret the  $S_{11}(1535)$  as a quasi-bound  $K\Lambda$ - $K\Sigma$  state [43]. Here, we will show that this is not necessarily the case.

In order to model the electromagnetic structure of  $B_{0+}$  and  $C_{0+}$ , we include monopole form factors  $(1 + Q^2/M_\alpha^2)^{-1}$  with a mass parameter  $M_\alpha$  depending on the outgoing channel  $\alpha$ . For  $\eta$  and  $\eta'$  electroproduction the channels  $|\pi N\rangle$  and  $|K\Lambda\rangle$  dominate the amplitude. We choose  $M_{|\pi N\rangle} = 0.6 \text{ GeV}$  for the first channel, so that the form factor is almost identical with the Dirac form factor of the proton, and  $M_{|K\Lambda\rangle} = 2.2 \text{ GeV}$  for the latter. The remaining three channels play only a minor role and we set  $M_\alpha = 1 \text{ GeV}$  in their case. The results for  $\eta$  and  $\eta'$  electroproduction after including these form factors are given in Fig. 9. Surprisingly, the cross sections for  $\eta$  electroproduction are increased, while they are reduced in the case of the  $\eta'$ .



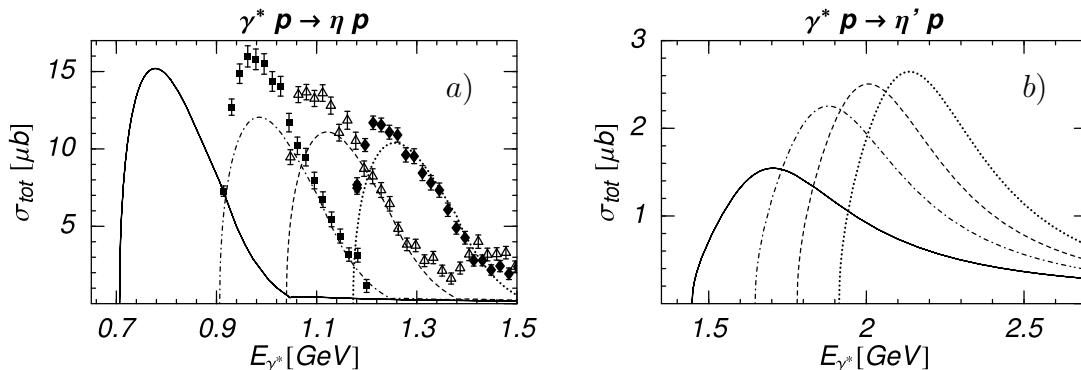


Figure 9: Cross sections for  $\eta$  and  $\eta'$  electroproduction on the proton after the inclusion of electromagnetic form factors for various invariant momentum transfers  $Q^2$ . The different lines refer to the following values of  $Q^2$ : solid line: photoproduction ( $Q^2 = 0$ ); dash-dotted line and squares:  $Q^2 = 0.375 \text{ GeV}^2$ ; dashed line and triangles:  $Q^2 = -0.625 \text{ GeV}^2$ ; dotted line and diamonds:  $Q^2 = 0.875 \text{ GeV}^2$ . The data for  $\eta$  electroproduction with the same  $Q^2$  values are taken from [13], and only statistical errors are shown.

This is due to the fact that we employed different form factors for the participating channels and that some of these channels may compensate each other in the final state interactions. To be more precise, for  $\eta$  electroproduction the  $|\pi N\rangle$  and  $|K\Lambda\rangle$  channels tend to counterbalance each other, for  $\eta'$  electroproduction, on the other hand, they add up. In contrast to common belief, the inclusion of form factors can increase the cross section, e.g. in  $\eta$  electroproduction, yielding a  $Q^2$  evolution closer to experiment and indicating a hard transition form factor. The claim that the hard form factor is counterintuitive to an interpretation of this state as a bound hadronic system [43] is not justified, since within the model the photon couples directly to one of the ground state octet baryons or a meson and only after this initial reaction the produced meson forms a bound state with the baryon.

We do not expect our results for electroproduction to reproduce precisely the experimental data. Nevertheless, the inclusion of simple form factors for the electroproduction potentials is able to explain qualitatively the slow decrease of the  $S_{11}(1535)$  photocoupling. The same form factors also flatten the increase in the  $Q^2$  evolution in  $\eta'$  electroproduction but keeping the results still above the cross section for photoproduction. Again, we cannot regard it as very likely that the results for the  $\eta'$  will be in exact agreement with future experimental data, in particular due to the uncertainties involved with the implemented form factors. The qualitative behavior of the  $Q^2$  evolution, however, indicates a hard transition form factor also for  $\eta'$  electroproduction. Within our model it would be very unlikely to accommodate both a hard form factor for  $\eta$  electroproduction and faster decreasing cross sections for electroproduction of the  $\eta'$ . Upcoming experiments will clarify this issue and provide a further test of the model.

Next, we consider  $\eta$  and  $\eta'$  electroproduction on the neutron, see Fig. 10. We have employed the same monopole form factors as in the case of the proton. Photoproduction of the  $\eta$  has a cross section of about  $6 \mu b$  at its peak, being less than half of the cross section on the proton. This ratio was measured to be approximately  $2/3$  [44] which is clearly above our prediction. This problem was already recognized in [17] and is due to the fact that the photon cannot couple directly via the charge to a neutral baryon or meson and thus some of the electroproduction amplitudes  $B_{0+}$  and  $C_{0+}$  vanish, e.g., the  $K\Lambda$  channel to the order we are working. To cure this problem, the leading corrections for the coupling of the photon to a neutral baryon via its

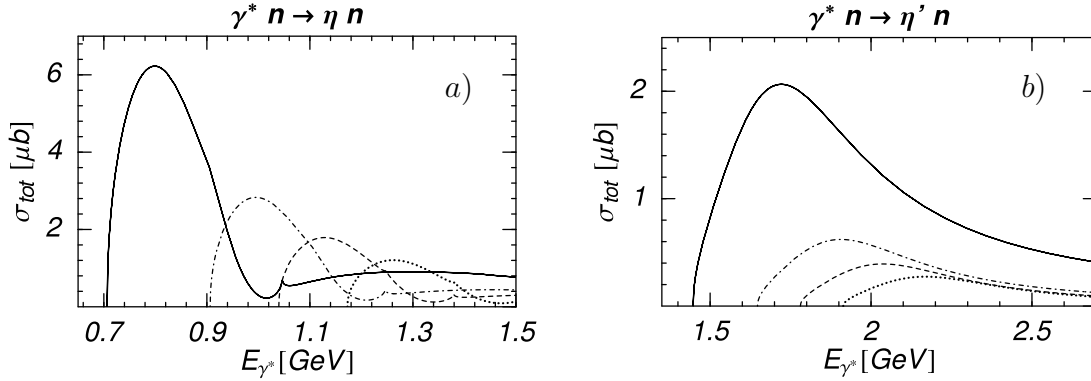


Figure 10: Cross sections for  $\eta$  and  $\eta'$  electroproduction on the neutron for various invariant momentum transfers  $Q^2$ . The different lines refer to the following values of  $Q^2$ : solid line: photoproduction ( $Q^2 = 0$ ); dash-dotted line:  $Q^2 = -0.375$  GeV<sup>2</sup>; dashed line:  $Q^2 = -0.625$  GeV<sup>2</sup>; dotted line:  $Q^2 = -0.875$  GeV<sup>2</sup>.

anomalous magnetic moment have been taken into account in [17] leading to better agreement with experiment. As these corrections originate from the higher order Lagrangian, which is beyond the scope of the present investigation, we refrain from including these terms, but keep in mind that sizable corrections may occur in electroproduction on the neutron. The  $Q^2$  evolution of the cross section exhibits a sharp decrease both for  $\eta$  and  $\eta'$ , a behavior which is remarkably different from the proton case and provides another prediction to be checked. This is due to the inclusion of form factors, otherwise the cross sections for  $\eta$  and  $\eta'$  electroproduction on the neutron, not shown here for brevity, would grow with  $Q^2$ .

### 5.3 Effects of the $\eta'$

In this section, we wish to investigate the effects of  $\eta$ - $\eta'$  mixing and the importance of the  $|\eta'N\rangle$  virtual state in our coupled channel formalism. This is done in a two-step procedure: first,  $\eta$ - $\eta'$  mixing is turned off, and secondly, we eliminate the  $|\eta'N\rangle$  channel from the model. In both cases we do not repeat the fit which would actually compensate most of the changes. We are particularly interested in the reaction  $\pi^-p \rightarrow K^0\Lambda$  which exhibits the most prominent  $\eta'N$  cusp of all the channels. Omission of both  $\eta$ - $\eta'$  mixing and the  $|\eta'N\rangle$  channel do not lead to substantial differences in the remaining reactions (where the  $\eta'$  is not produced). In Fig. 11 we have chosen to present in addition to  $\pi^-p \rightarrow K^0\Lambda$  the photoproduction process  $\gamma p \rightarrow \eta p$ , in order to give a measure for the changes in the other channels. For  $\pi^-p \rightarrow K^0\Lambda$  variation in  $\eta$ - $\eta'$  mixing has almost no impact (dash-dotted line), like in most other channels in which the  $\eta$  is not produced as a final particle. Eliminating the  $|\eta'N\rangle$  channel makes the  $\eta'N$  cusp disappear and lowers the cross section, bringing it to better agreement with the data (dashed line). It suggests that the region around the  $\eta'N$  cusp is overemphasized within our model. This feature may change after the inclusion of  $p$ -waves, since then a new overall fit to the different reaction channels will lower the  $s$ -wave contribution reducing the absolute importance of the cusp. For the photoproduction of the  $\eta$  on the proton  $\eta$ - $\eta'$  mixing plays a slightly more prominent role (dash-dotted line), as the  $\eta$  is produced in the final state. If the  $|\eta'N\rangle$  channel is turned off, the changes are again quite moderate (dashed line). Overall we can conclude, that the results for the production of the Goldstone bosons are not modified substantially after omitting the  $\eta'$  which is in accordance with intuitive expectation, since the  $|\eta'N\rangle$  channel is much higher

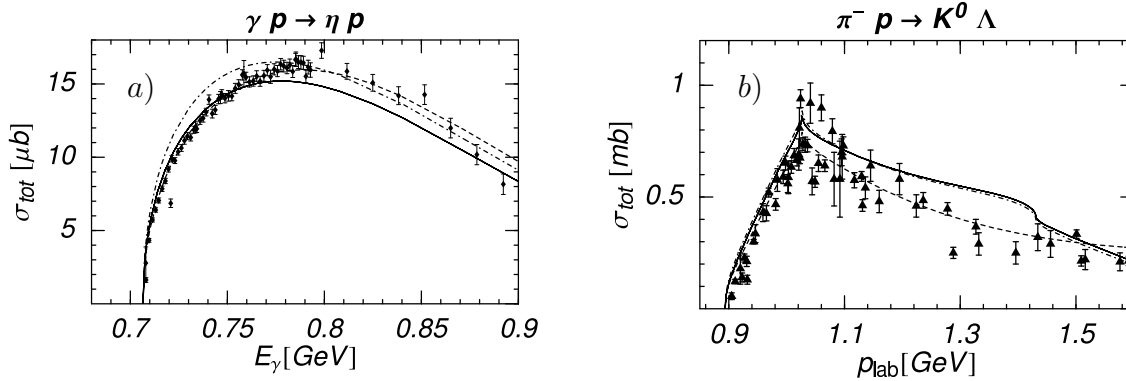


Figure 11: Shown are the differences in the cross sections for  $\gamma p \rightarrow \eta p$  and  $\pi^- p \rightarrow K^0 \Lambda$  after neglecting  $\eta$ - $\eta'$  mixing and the  $|\eta' N\rangle$  channel in the coupled channel formalism. The solid line is the original result, the dash-dotted line is obtained for vanishing  $\eta$ - $\eta'$  mixing, and the dashed line refers to the case without the  $|\eta' N\rangle$  channel.

in mass than the other channels. We can therefore confirm that it was justified in previous coupled channel analyses to neglect  $\eta$ - $\eta'$  mixing and treat the  $\eta$  as a pure octet state, see e.g. [17].

## 6 Conclusions

In this work we presented a coupled channel approach to meson-baryon scattering and electroproduction processes including the  $\eta'$  meson based on chiral symmetry and unitarity. Since we restrict ourselves to the threshold region, only  $s$ -wave contributions are taken into account which are dominant at the pertinent energies for most of the discussed reactions. The most general chiral effective Lagrangian for the strong interactions which includes the  $\eta'$  explicitly is presented up to next-to-leading order and the effective  $s$ -wave potentials are derived which are then iterated in a Bethe-Salpeter equation. Following the work of [17] we extended the formalism to include electroproduction processes where the photon can couple to the hadrons via their charge.

With only a few chiral parameters –these are, on the one hand, the unknown coupling constants of the Lagrangian and, on the other hand, the regularization scales of the loop integrals within the Bethe-Salpeter equation– we performed a fit to a large amount of data, consisting of meson-baryon scattering and photoproduction of mesons on the proton. The  $s$ -wave approximation yields good agreement with the low-energy data in many channels, whereas in the remaining channels  $p$ -wave contributions are expected to be dominant. We clearly generate the appearance of the  $S_{11}(1535)$  in the pion- and photo-induced production of the  $\eta$ , while the  $S_{11}(1650)$  is produced in the  $K\Lambda$  channels. We are also able to produce a resonance-like shape in the photoproduction of the  $\eta'$  which has been assigned to the  $S_{11}(1897)$  in a recent experiment at ELSA. The overall agreement of our results with data indicates that chiral dynamics and unitarity govern processes up to center-of-mass energies of  $\sqrt{s} = 2$  GeV and that the  $\eta'$  can be included systematically in a chiral effective Lagrangian with baryons.

Having constrained the parameters of the approach, we can give predictions for further processes such as the pion-induced production of the  $\eta'$  in  $\pi^- p \rightarrow \eta' n$  or  $\eta$  and  $\eta'$  electroproduction, which is more sensitive to the structures of the nucleon due to the longitudinal coupling of the

virtual photon to the nucleon spin and provides a better test for our model when compared with data. The only available electroproduction data exists so far for the  $\eta$  with invariant momentum transfers  $Q^2$  starting at 0.375 GeV<sup>2</sup>. It exhibits an unusually slow  $Q^2$  evolution which is in general difficult to understand. Although our results are larger than that of a simple nucleon dipole form factor, for example, they exhibit a faster decrease with  $Q^2$  for small values of  $Q^2$  which then flattens at higher momentum transfers. In the case of  $\eta'$  electroproduction, the features of the  $Q^2$  evolution of the cross section are even more striking, since they exhibit a fast increase instead of the usual decrease. By choosing different form factors for the initial electroproduction potentials which take into account the electromagnetic structure of the hadrons instead of treating them as pointlike particles the cross sections for  $\eta$  electroproduction are *increased*, but lowered for the  $\eta'$ . This brings the  $Q^2$  evolution of  $\eta$  electroproduction closer to experiment and signals a hard transition form factor within the model. We argue that according to this approach a hard form factor is expected also for  $\eta'$  electroproduction which provides a further test of the model. In order to make more precise statements, one must include not only  $p$ -waves, but also higher order corrections for the coupling of the photon to a baryon via its anomalous magnetic moment. The omission of such contact interactions explains why we fail in reproducing the photoproduction cross section of the  $\eta$  on the neutron.

Finally, we have discussed the impact of  $\eta$ - $\eta'$  mixing and the importance of the  $|\eta'N\rangle$  channel within the coupled channel formalism. Omission of the mixing and the  $|\eta'N\rangle$  channel do not lead to substantial changes in those reactions in which the  $\eta'$  is not produced as a final particle. This is in accordance with intuitive expectation, since the  $|\eta'N\rangle$  channel is much higher in mass than the other channels.

## Acknowledgements

We are grateful to N. Kaiser who shared his insight in the coupled channel formalism with us. Useful discussions with T. Hemmert and W. Weise are gratefully acknowledged. We would also like to thank J. Mueller for providing us with the data for  $\eta$  electroproduction from CLAS at JLab. This work has been supported in part by the Deutsche Forschungsgemeinschaft.

## A

In this appendix, we list the coefficients  $C_\alpha^\beta(s)$  from Eq. (16) in the isospin basis. There are five channels with total isospin  $I = 1/2$  which are  $|\pi N\rangle^{(1/2)}$ ,  $|\eta N\rangle^{(1/2)}$ ,  $|K\Lambda\rangle^{(1/2)}$ ,  $|K\Sigma\rangle^{(1/2)}$ ,  $|\eta'N\rangle^{(1/2)}$  (labelled with indices 1, 2, 3, 4, 5, respectively) and two channels with  $I = 3/2$ ,  $|\pi N\rangle^{(3/2)}$ ,  $|K\Sigma\rangle^{(3/2)}$  (labeled by indices 6 and 7). The physical states can be expressed in terms

of the isospin states,

$$\begin{aligned}
|\pi^+ n\rangle &= \frac{1}{\sqrt{3}} \left( \sqrt{2} |\pi N\rangle^{(1/2)} + |\pi N\rangle^{(3/2)} \right) \\
|\pi^0 p\rangle &= \frac{1}{\sqrt{3}} \left( |\pi N\rangle^{(1/2)} - \sqrt{2} |\pi N\rangle^{(3/2)} \right) \\
|K^+ \Sigma^0\rangle &= \frac{1}{\sqrt{3}} \left( |K \Sigma\rangle^{(1/2)} - \sqrt{2} |K \Sigma\rangle^{(3/2)} \right) \\
|K^+ \Sigma^-\rangle &= \frac{1}{\sqrt{3}} \left( \sqrt{2} |K \Sigma\rangle^{(1/2)} - |K \Sigma\rangle^{(3/2)} \right) \\
|K^0 \Sigma^+\rangle &= \frac{1}{\sqrt{3}} \left( \sqrt{2} |K \Sigma\rangle^{(1/2)} + |K \Sigma\rangle^{(3/2)} \right) \\
|K^0 \Sigma^0\rangle &= \frac{1}{\sqrt{3}} \left( -|K \Sigma\rangle^{(1/2)} - \sqrt{2} |K \Sigma\rangle^{(3/2)} \right), \tag{A.1}
\end{aligned}$$

where we have used the convention in which for the following states there is a sign difference between the physical and isospin basis:  $|\pi^+\rangle = -|1, 1\rangle$ ,  $|K^+\rangle = -|1/2, 1/2\rangle$ ,  $|K^0\rangle = -|1/2, -1/2\rangle$ ,  $|\bar{K}^0\rangle = -|1/2, 1/2\rangle$ ,  $|\Sigma^+\rangle = -|1, 1\rangle$ ,  $|p\rangle = -|1/2, 1/2\rangle$ ,  $|n\rangle = -|1/2, -1/2\rangle$ ,  $|\Xi^0\rangle = -|1/2, 1, 2\rangle$ .

The octet field  $\eta_8$  and its singlet counterpart  $\eta_0$  as they appear in the Lagrangian are related to the physical mass eigenstates  $\eta$  and  $\eta'$  in the one-mixing-angle scheme as follows

$$\begin{aligned}
\eta_8 &= \eta \cos \vartheta + \eta' \sin \vartheta \\
\eta_0 &= -\eta \sin \vartheta + \eta' \cos \vartheta, \tag{A.2}
\end{aligned}$$

where we have used  $\vartheta = -10^\circ$ . This is the value which one obtains from the Gell-Mann–Okubo mass relation for the pseudoscalar mesons at lowest order. As discussed in the main text, small variations in this value lead only to moderate changes which can even be partially compensated by repeating the fit. The implementation of the more general two-mixing-angle scheme, see e.g. [28], does not change any of our conclusions and will therefore not be considered here.

The coefficients  $C_i^j$  read

$$\begin{aligned}
C_1^1 &= \sqrt{s} - M_N - \frac{3}{4}(D + F)^2 \frac{(\sqrt{s} - M_N)^2}{\sqrt{s} + M_N} \\
&\quad - 2(2b_0 + b_D + b_F)m_\pi^2 + 2(d_1 + d_2 + 2d_4)P_1^1 \\
C_1^2 &= -\frac{1}{4}(D + F) \left( \sqrt{2}(2D + 3D_s) \sin \vartheta + (D - 3F) \cos \vartheta \right) \frac{(\sqrt{s} - M_N)^2}{\sqrt{s} + M_N} \\
&\quad + 2 \left( [b_D + b_F] \cos \vartheta - [\sqrt{2}(b_D + b_F) - \sqrt{3}(c_D + c_F)] \sin \vartheta \right) m_\pi^2 \\
&\quad - \left( 2[d_1 + 3d_2] \cos \vartheta - \sqrt{2}[2d_1 + 3d_5 + 3d_6] \sin \vartheta \right) P_1^2 \\
C_1^3 &= -\frac{3}{8}[M_N + M_\Lambda - 2\sqrt{s}] - \frac{1}{4}(D + F)(D + 3F) \frac{(\sqrt{s} - M_N)(\sqrt{s} - M_\Lambda)}{\sqrt{s} + M_N} \\
&\quad - \frac{1}{2}(b_D + 3b_F)(m_K^2 + m_\pi^2) + 3(d_1 + d_2)P_1^3 \\
C_1^4 &= -\frac{1}{8}[M_N + M_\Sigma - 2\sqrt{s}] - \frac{3}{4}(D^2 - F^2) \frac{(\sqrt{s} - M_N)(\sqrt{s} - M_\Sigma)}{\sqrt{s} + M_N} \\
&\quad + \frac{1}{2}(b_D - b_F)(m_K^2 + m_\pi^2) + (d_1 - 7d_2 + 2d_3)P_1^4 \\
C_1^5 &= \frac{1}{4}(D + F) \left( \sqrt{2}(2D + 3D_s) \cos \vartheta - (D - 3F) \sin \vartheta \right) \frac{(\sqrt{s} - M_N)^2}{\sqrt{s} + M_N} \\
&\quad + 2 \left( [b_D + b_F] \sin \vartheta + [\sqrt{2}(b_D + b_F) - \sqrt{3}(c_D + c_F)] \cos \vartheta \right) m_\pi^2 \\
&\quad - \left( \sqrt{2}[2d_1 + 3d_5 + 3d_6] \cos \vartheta + 2[d_1 + 3d_2] \sin \vartheta \right) P_1^5 \\
C_2^2 &= -\frac{1}{12} \left( \sqrt{2}(2D + 3D_s) \sin \vartheta + (D - 3F) \cos \vartheta \right)^2 \frac{(\sqrt{s} - M_N)^2}{\sqrt{s} + M_N} - 4M_N u_1 \sin^2 \vartheta \\
&\quad + \frac{8}{3} \left( -[b_0 + b_D - b_F] (\sqrt{2} \cos \vartheta + \sin \vartheta)^2 + \sqrt{6}[c_0 + c_D - c_F] \sin \vartheta (\sqrt{2} \cos \vartheta + \sin \vartheta) \right) m_K^2 \\
&\quad + \frac{2}{3} \left( [2b_0 + 3b_D - 5b_F] \cos^2 \vartheta - 2[\sqrt{2}(-4b_0 - 3b_D + b_F) + \sqrt{3}(4c_0 + 3c_D - c_F)] \cos \vartheta \sin \vartheta \right. \\
&\quad \left. - \frac{4}{3}[b_0 + 2b_F - \sqrt{6}(c_0 + 2c_F)] \sin^2 \vartheta \right) m_\pi^2 \\
&\quad + 2 \left( 2[d_4 + 2d_5 + 3d_7] \sin^2 \vartheta - \sqrt{2}[2d_1 - d_5 + 3d_6] \sin \vartheta \cos \vartheta + [-d_1 + 3d_2 + 2d_4] \cos^2 \vartheta \right) P_2^2
\end{aligned}$$

$$\begin{aligned}
C_2^3 &= \frac{3}{8}[M_N + M_\Lambda - 2\sqrt{s}] \cos \vartheta \\
&\quad - \frac{1}{12}(D + 3F) \left( \sqrt{2}(2D + 3D_s) \sin \vartheta + (D - 3F) \cos \vartheta \right) \frac{(\sqrt{s} - M_N)(\sqrt{s} - M_\Lambda)}{\sqrt{s} + M_N} \\
&\quad + \frac{1}{6}[b_D + 3b_F](3m_\pi^2 - 5m_K^2) \cos \vartheta - \frac{2}{3}[\sqrt{2}(b_D + 3b_F) - \sqrt{3}(c_D + 3c_F)]m_K^2 \sin \vartheta \\
&\quad + \left( \sqrt{2}[2d_1 + d_5 + 3d_6] \sin \vartheta + [d_1 - 3d_2 + 2d_3] \cos \vartheta \right) P_2^3 \\
C_2^4 &= \frac{3}{8}[2\sqrt{s} - M_N - M_\Sigma] \cos \vartheta \\
&\quad - \frac{1}{4}(D - F) \left( \sqrt{2}(2D + 3D_s) \sin \vartheta + (D - 3F) \cos \vartheta \right) \frac{(\sqrt{s} - M_N)(\sqrt{s} - M_\Sigma)}{\sqrt{s} + M_N} \\
&\quad + \frac{1}{2}[b_D - b_F](3m_\pi^2 - 5m_K^2) \cos \vartheta - 2[\sqrt{2}(b_D - b_F) - \sqrt{3}(c_D - c_F)]m_K^2 \sin \vartheta \\
&\quad - \left( \sqrt{2}[2d_1 - 3d_5 + 3d_6] \sin \vartheta + [d_1 - 3d_2] \cos \vartheta \right) P_2^4 \\
C_2^5 &= \frac{1}{12} \left( \sqrt{2}(2D + 3D_s) \sin \vartheta + (D - 3F) \cos \vartheta \right) \left( \sqrt{2}(2D + 3D_s) \cos \vartheta - (D - 3F) \sin \vartheta \right) \\
&\quad \times \frac{(\sqrt{s} - M_N)^2}{\sqrt{s} + M_N} + 4M_N u_1 \cos \vartheta \sin \vartheta \\
&\quad + \frac{1}{3} \left[ \left( 8\sqrt{2}(b_0 + b_D - b_F) - 8\sqrt{3}(c_0 + c_D - c_F) \right) m_K^2 \right. \\
&\quad \left. - \left( 2\sqrt{2}(4b_0 + 3b_D - b_F) - 2\sqrt{3}(4c_0 + 3c_D - c_F) \right) m_\pi^2 \right. \\
&\quad \left. + 3\sqrt{2}(2d_1 - d_5 + 3d_6) P_2^5 \right] \cos(2\vartheta) \\
&\quad - \frac{1}{3} \left[ 4 \left( b_0 + b_D - b_F + \sqrt{6}(c_0 + c_D - c_F) \right) m_K^2 \right. \\
&\quad \left. + \left( -4b_0 - 3b_D + b_F + 2\sqrt{6}(c_0 + 2c_F) \right) m_\pi^2 \right. \\
&\quad \left. + 3(d_1 - 3d_2 + 4d_5 + 6d_7) P_2^5 \right] \sin(2\vartheta) \tag{A.3}
\end{aligned}$$

$$\begin{aligned}
C_3^3 &= -\frac{1}{12}(D+3F)^2 \frac{(\sqrt{s}-M_\Lambda)^2}{\sqrt{s}+M_N} \\
&\quad -\frac{2}{3}(6b_0+5b_D)m_K^2 + 2(3d_2+2d_4)P_3^3 \\
C_3^4 &= -\frac{1}{4}(D-F)(D-3F) \frac{(\sqrt{s}-M_\Sigma)(\sqrt{s}-M_\Lambda)}{\sqrt{s}+M_N} \\
&\quad + 2b_D m_K^2 - 6d_2 P_3^4 \\
C_3^5 &= \frac{3}{8}[M_N+M_\Lambda-2\sqrt{s}] \sin \vartheta \\
&\quad + \frac{1}{12}(D+3F) \left( \sqrt{2}(2D+3D_s) \cos \vartheta - (D-3F) \sin \vartheta \right) \frac{(\sqrt{s}-M_N)(\sqrt{s}-M_\Lambda)}{\sqrt{s}+M_N} \\
&\quad + \frac{1}{6}[b_D+3b_F](3m_\pi^2-5m_K^2) \sin \vartheta + \frac{2}{3}[\sqrt{2}(b_D+3b_F)-\sqrt{3}(c_D+3c_F)]m_K^2 \cos \vartheta \\
&\quad - \left( \sqrt{2}[2d_1+d_5+3d_6] \cos \vartheta - [d_1-3d_2+2d_3] \sin \vartheta \right) P_3^5 \\
C_4^4 &= \sqrt{s}-M_\Sigma - \frac{3}{4}(D-F)^2 \frac{(\sqrt{s}-M_\Sigma)^2}{\sqrt{s}+M_N} \\
&\quad - 2(2b_0+b_D-2b_F)m_K^2 + 2(-2d_1+d_2+2d_4)P_4^4 \\
C_4^5 &= \frac{3}{8}[2\sqrt{s}-M_N-M_\Sigma] \sin \vartheta \\
&\quad + \frac{1}{4}(D-F) \left( \sqrt{2}(2D+3D_s) \cos \vartheta - (D-3F) \sin \vartheta \right) \frac{(\sqrt{s}-M_N)(\sqrt{s}-M_\Sigma)}{\sqrt{s}+M_N} \\
&\quad + \frac{1}{2}[b_D-b_F](3m_\pi^2-5m_K^2) \sin \vartheta + 2[\sqrt{2}(b_D-b_F)-\sqrt{3}(c_D-c_F)]m_K^2 \cos \vartheta \\
&\quad + \left( \sqrt{2}[2d_1-3d_5+3d_6] \cos \vartheta - [d_1-3d_2] \sin \vartheta \right) P_4^5 \\
C_5^5 &= -\frac{1}{12} \left( \sqrt{2}(2D+3D_s) \cos \vartheta - (D-3F) \sin \vartheta \right)^2 \frac{(\sqrt{s}-M_N)^2}{\sqrt{s}+M_N} - 4M_N u_1 \cos^2 \vartheta \\
&\quad + \frac{8}{3} \left( -[b_0+b_D-b_F](\sqrt{2} \sin \vartheta - \cos \vartheta)^2 - \sqrt{6}[c_0+c_D-c_F] \cos \vartheta (\sqrt{2} \sin \vartheta - \cos \vartheta) \right) m_K^2 \\
&\quad + \frac{2}{3} \left( [2b_0+3b_D-5b_F] \sin^2 \vartheta + 2[\sqrt{2}(-4b_0-3b_D+b_F)+\sqrt{3}(4c_0+3c_D-c_F)] \sin \vartheta \cos \vartheta \right. \\
&\quad \left. - 2[b_0+2b_F-\sqrt{6}(c_0+2c_F)] \cos^2 \vartheta \right) m_\pi^2 \\
&\quad + 2 \left( 2[d_4+2d_5+3d_7] \cos^2 \vartheta + \sqrt{2}[2d_1-d_5+3d_6] \cos \vartheta \sin \vartheta + [-d_1+3d_2+2d_4] \sin^2 \vartheta \right) P_5^5 \\
C_6^6 &= -\frac{1}{2}[\sqrt{s}-M_N] - 2(2b_0+b_D+b_F)m_\pi^2 + 2(d_1+d_2+2d_4)P_6^6 \\
C_6^7 &= \frac{1}{4}[M_N+M_\Sigma-2\sqrt{s}] - (b_D-b_F)(m_K^2+m_\pi^2) + 2(-d_1+d_2+d_3)P_6^7 \\
C_7^7 &= -\frac{1}{2}[\sqrt{s}-M_\Sigma] - 2(2b_0+b_D+b_F)m_K^2 + 2(d_1+d_2+2d_4)P_7^7
\end{aligned}$$



For an isospin state labeled  $\alpha$  ( $\beta$ ) which consists of a baryon  $a$  ( $b$ ) and a meson  $i$  ( $j$ ) we have used the abbreviation

$$P_\alpha^\beta = E_i E_j + \frac{|\mathbf{p}|^2 |\mathbf{p}'|^2}{3N_a^2 N_b^2}. \quad (\text{A.4})$$

The energies of the mesons are given by  $E_{i(j)}$  and  $\mathbf{p}$  ( $\mathbf{p}'$ ) is the three-momentum of the incoming (outgoing) baryon in the center-of-mass frame.

## References

- [1] N. Kaiser, P. B. Siegel, W. Weise, Nucl. Phys. **A594** (1995) 325
- [2] N. Kaiser, P. B. Siegel, W. Weise, Phys. Lett. **B362** (1995) 23
- [3] J. A. Oller, E. Oset, Nucl. Phys. **A620** (1997) 438;  
J. A. Oller, E. Oset, J. R. Peláez, Phys. Rev. **D59** (1999) 074001
- [4] E. Oset, A. Ramos, Nucl. Phys. **A635** (1998) 99
- [5] J. A. Oller, U.-G. Meißner, Phys. Lett. **B500** (2001) 263
- [6] T. Inoue, E. Oset, M. J. Vicente Vacas, Phys. Rev. **C65** (2002) 035204
- [7] B. Krusche et al., Phys. Rev. Lett. **74** (1995) 3736
- [8] B. Schoch, Prog. Part. Nucl. Phys. **35** (1995) 43
- [9] C. E. Carlson, J. L. Poor, Phys. Rev. **D38** (1988) 2758
- [10] D. B. Leinweber, T. Draper, R. M. Woloshyn, Phys. Rev. **D46** (1992) 3067
- [11] V. V. Frolov et al., Phys. Rev. Lett. **82**, (1999) 45
- [12] C. S. Armstrong et al., Phys. Rev. **D60**, (1999) 052004
- [13] R. Thompson et al., Phys. Rev. Lett. **86**, (2001) 1702
- [14] M. Benmerrouche, N. C. Mukhopadhyay, Phys. Rev. Lett. **67** (1991) 1070;  
M. Benmerrouche, N. C. Mukhopadhyay, J. F. Zhang, Phys. Rev. **D51** (1995) 3237
- [15] C. Bennhold, H. Tanabe, Nucl. Phys. **A530** (1991) 625
- [16] L. Tiator, C. Bennhold, S.S. Kamalov, Nucl. Phys. **A580** (1994) 455
- [17] N. Kaiser, T. Waas, W. Weise, Nucl. Phys. **A612** (1997) 297;  
J. Caro Ramon, N. Kaiser, S. Wetzel, W. Weise, Nucl. Phys. **A672** (2000) 249
- [18] S. Weinberg, Phys. Rev. **D11** (1975) 3583
- [19] H. Leutwyler, Phys. Lett. **B374** (1996) 163
- [20] P. Herrera-Siklody, J. I. Latorre, P. Pascual and J. Taron, Nucl. Phys. **B497** (1997) 345

- [21] B. Borasoy, Phys. Rev. **D61** (2000) 014011
- [22] J. F. Zhang, N. C. Mukhopadhyay, M. Benmerrouche, Phys. Rev. **C52** (1995) 1134
- [23] Z. Li, J. Phys. **G23** (1997) 1127
- [24] S. D. Bass, S. Wetzell, and W. Weise, Nucl. Phys. **A686** (2001) 429
- [25] R. Plötzke et al., Phys. Lett. **B444** (1998) 555
- [26] B. Norum, private communication;  
E. Pasyuk, private communication
- [27] R. Kaiser, H. Leutwyler, Eur. Phys. J. **C17** (2000) 623
- [28] N. Beisert, B. Borasoy, Eur. Phys. J. **A11** (2001) 329
- [29] F. E. Close, R. G. Roberts, Phys. Lett. **B316** (1993) 165;  
B. Borasoy, Phys. Rev. **D 59** (1999) 054021
- [30] M. Gell-Mann, Phys. Rev. **125** (1962) 1067;  
S. Okubo, Prog. Theor. Phys. **27** (1962) 949
- [31] J. Gasser, H. Leutwyler, M.E. Sainio, Phys.Lett. **B253** (1991) 252
- [32] M.M. Pavan, I.I. Strakovsky, R.L. Workman, R.A. Arndt, ” *The pion nucleon sigma term is definitely large: results from a G.W.U. analysis of pion nucleon scattering data.*”, hep-ph/0111066
- [33] B. Borasoy, U.-G. Meißner, Ann. Phys. (NY) **254** (1997) 192
- [34] N. Beisert, B. Borasoy, Nucl. Phys. **A705** (2002) 433
- [35] T. Feldmann, P. Kroll, Eur. Phys. J. **C5** (1998) 327
- [36] T. Becher, H. Leutwyler, Eur. Phys. J. **C9** (1999) 643
- [37] J. Nieves and E. Ruiz Arriola, Nucl. Phys. **A679** (2000) 57
- [38] B. Borasoy, Phys. Rev. **D63**, (2001) 094015
- [39] A. Baldini et al., in: Landolt-Börnstein (Ed.), Vol. 12a, Springer, Berlin, 1988
- [40] M. Q. Tran et al. (SAPHIR Collaboration), Phys. Lett. **B445** (1998) 20
- [41] S. Goers et al. (SAPHIR Collaboration), Phys. Lett. **B464** (1999) 331
- [42] M. M. Giannini, E. Santopinto, A. Vasallo, Nucl. Phys. **A699** (2002) 308
- [43] V. D. Burkert, Talk presented at Baryons 2002, Newport News, USA, to appear in the proceedings; hep-ph/0207149
- [44] P. Hoffmann-Rothe et al., Phys. Rev. Lett. **78** (1997) 4697